International Journal on Science and Technology (IJSAT)
E-ISSN: 2229-7677 ● Website: www.ijsat.org ● Email: editor@ijsat.org

Concentration-Dependent Photoluminescence & Thermoluminescence Properties of Eu^{3+} Doped CaF_2 Phosphors

Usha Yadav[1], Jagjeet Kaur[2], Abhishek Kumar Misra[3]

[1,2,3]Department of Physics, Govt. V.Y.T. PG Autonomous College Durg C.G.

Abstract

In the present study conventional solid state reaction method was used to successfully synthesize a series of Eu^{3+} doped CaF_2 phosphors for 0.1- 2.5 mol% of Eu^{3+} ions. In this study investigate its structural, vibration and optical properties. X-ray diffraction analysis confirms the phase purity and crystalline nature of the prepared phosphor and which revealed a cubic structure without any detectable impurity phases. The FTIR (Fourier Transform Infrared Spectroscopy) is used to examine the vibrational characteristics and bonding nature of the prepared sample. Under the UV excitation Eu^{3+} doped CaF_2 phosphor demonstrate strong emission in visible spectrum, specially while the photoluminescence excitation peaked at 280 nm, in the emission spectra broad band centered at 611 nm($^5D_0 \rightarrow {}^7F_2$), due to the electronic transitions of Eu^{3+} ions. While literature reports on chemically synthesized CaF_2:Eu^{3+} often exhibit early concentration quenching or require co-doping to enhance intensity but we observed in the present study PL intensity significantly influenced by the activator (Eu^{3+}), the emission intensity increases with rise concentration of Eu^{3+} ion up to 2.0 mol%, after that concentration quenching occurs, which is relatively high concentration of 2.0 mol%. Most significantly, thermoluminescence (TL) studies revealed a well-defined glow peak, indicating the presence of trapping centers linked to Eu^{3+} ions. Compared to commercial dosimeters, the synthesized phosphor has highest intensity recorded at a 0.1 kGy dose for 1.5 mol% sample, the kinetic parameters such as, frequency factor, activation energy and order of kinetics calculated using peak shape method. These comparative findings establish this phosphor as a more robust and highly promising for application in LED technology and highly sensitive alternative for advanced radiation dosimetry applications.

Keywords: Solid state, CaF_2, Eu^{3+}, PL, TL & LEDs.

1.Introduction

Over the past few years, rare-earth-doped fluoride phosphors have gained significant interest due to their remarkable luminescence efficiency, these characteristics make them highly suitable for a wide range of display applications. Consequently, these materials are now extensively used as emissive components in various devices such as field effect transistors (FETs), Cathode ray tubes (CRTs) and light emitting diodes (LEDs). Specifically, fluoride-based phosphors are essential for studying advanced thermoluminescence and photoluminescence properties. When compared to traditional light sources like fluorescent lamp and incandescent bulb, LED offer clear advantage, including enhanced operational life, superior energy

efficiency and environmental compatibility. These make them a highly sustainable for future lighting solutions, furthermore in the research and innovation field has led to increased automation in daily life, simplifying human tasks and offering greater convenience through advanced, technology driven system. The concept of lifestyle managed simply by the push of button- made possible by growing automation – points towards a future of seamless efficiency, as research continue advance the integration of these smart technologies into our daily life routines is becoming more mechanization. This evolution not only reduces manual effort but also enhances the overall quality of life by making complex systems more accessible and user friendly. Ultimately, the progress in material science, such as the development of efficient phosphors, plays a silent but vital role in powering the hardware that drives this automated world. To detecting or reporting to external stimuli these smart materials are a capable substance, these stimuli may encompass a variety of types, include environmental, optical, electrical, thermal, biological, and chemical changes[1–4]. The miniaturization of display systems has heightened research interest in luminescent materials[5–7]. The applications of advanced light emitting phosphors are extensive, encompassing polymeric optical fibers, LEDs, displays, and light sensors[8–12]. Next-generation smart materials must balance mechanical robustness with flexibility to ensure reliable performance in flexible devices, flexibility of the electronics these materials used in flexible electronic devices without compromising performance is a critical challenge for smart materials[13–18].The challenge presented is effectively addressed through the application of nanotechnology[19–22]. Consequently, the intrinsic luminescence characteristic is the primary attention of this investigation.This property holds potential for utilization in intelligent materials, particularly in the context of flexible display applications. Europium ($Eu^{3+)}$ doped CaF_2 has emerged as a significant luminescent material, primarily due to it is recognized as a prominent luminescent material, due to its intense and lasting red emission when triggered by ultraviolet light. The unique electronic transitions of Eu^{3+} ions are responsible for these distinct luminescent properties. CaF_2 is particularly suitable as host material because it offers excellent color purity in the red spectrum, however the practical application of these several factors such as raw material availability and manufacturing complexity. Notably, Eu^{3+}: CaF_2 phosphors exhibit remarkable thermal and chemical stability, ensuring consistent performance even under the demanding conditions typical of solid-state lighting. Furthermore, their extended operational life makes them ideal for long-term use. This study details an accessible method for synthesizing Eu^{3+} doped CaF_2 nanostructured phosphors and investigates how varying Eu^{3+} concentrations influence the particle size and morphology of the host lattice. The stability and longevity of phosphors are critical considerations in practical application. Furthermore, it offers an extended operational lifetime, ensuring consistent performance over prolonged periods. The intense emission line produced by the Eu^{3+} long-lasting transition $^5D_0 \rightarrow {}^7F_2$ of Eu^{3+} ions may be seen, at a wavelength of 611 nm, when the excitation of 280 nm (UV region), europium ions serve as very useful luminescent phosphors making them highly suitable for applications in display engineering. [24–36] In this work, we define how to simply make new CaF_2: Eu^{3+} phosphors and CaF_2:Eu^{3+} phosphor exhibits luminescent properties, which may be used to improve the attractive performance of smart materials for flexible displaying applications.

In this study, CaF_2 nanostructured particles were doped with Eu^{3+} ions. The effect of dopant ions Eu^{3+} concentration on the shape and particle size of CaF_2 was also studied. CaF_2:Eu^{3+} doped samples were synthesized by the solid-state reaction method. The structural and optical properties of synthesized nanostructured materials were studies using XRD X-Ray powder diffraction, FTIR and PL photoluminescence, TL thermoluminescence analysis and over the last few years, rare- earth ion (Eu)

doped fluoride phosphors have gained significant attention for display applications, including LEDs, CRTs and FETs due to their high quantum efficiency, among the various alkali fluorides, Calcium Fluoride(CaF_2) stands out due to its exceptional stability, nonhygroscopic nature, low refractive index and minimal phonon energy, making it an ideal host for a broad range of emitting ions.

2.Method of Synthesis

In this research, Eu^{3+}doped CaF_2 phosphors were prepared using a conventional solid - state reaction technique. In this approach, the initial raw materials, to achieve the desired composition of CaF_2:Eu^{3+}, CaF_2 and Eu_2O_3 are weighed and mixed in stoichiometric amounts, to ensure the homogenous mixture, it mixed together after weighing the starting raw material and ground together using mortar and pestle for a continuous period of two hours. The resulting fine mixture was then transferred to a furnace for an initial calcination stage at temperature 450ºC for one hour, after calcination the mixture of the powders again grind for 1 hour to improve uniformity and reduce particle agglomeration. The homogenized powder was then sintered again at 750 °C for 3 hours under the same atmospheric conditions to finalize the Eu^{3+} doped CaF_2 phosphor formation. After successful synthesis, to confirm the properties such as crystal structure, morphology, functional group analysis, we analysed the samples using different technique such as XRD & FTIR and also luminescence properties such as PL and TL studies. Fourier transform infrared (FTIR) spectroscopy was employed to identify the functional groups and bonding characteristics. The optical properties of the phosphor were investigated through photoluminescence (PL) spectroscopy, including excitation and emission measurements.

3.Results and discussion

3.1 X- Ray Diffraction Analysis

The X-ray diffraction (XRD) pattern of CaF_2:Eu^{3+}phosphor, synthesized via the solid-state reaction method, is depicted in **Fig**.1(a). XRD is commonly used technique which is involves shining a beam of X-ray on the sample, measuring the angle and intensity of the diffracted ray. The pattern exhibits several diffracted peaks with hkl values, indicating a fully crystalline structure in a cubic phase, as referenced by JCPDS Card number 35-0816. The observed peaks, corresponding to the values (1 1 1), (2 2 0), (3 1 1), (4 0 0), (3 3 1), and (4 2 2), confirm the formation of a pure cubic crystal structure, the X-ray diffraction pattern reveals broad peaks, indicative of the small crystallite size of the synthesized samples and the crystallite size was calculated from the full width at half maximum (FWHM) of all peaks in the XRD pattern using the Scherrer formula, expressed as:

$$D = k\lambda/\beta \, Cos\theta$$

Here, *D* represents the crystallite size perpendicular to the reflecting planes, $\lambda = 0.154$ nm represents the wavelength of the X-ray radiation, θ corresponds to the diffraction angle, and β indicates the full width at half maximum (FWHM) of the diffraction peak. Table 1 presents the values of diffraction angle, crystallite size, and FWHM for the synthesized sample. The crystallite size calculated from the most prominent peak in the XRD pattern of the CaF_2: Eu^{3+} phosphor was observed to be 29.31 nm, indicating that the prepared CaF_2 exhibits a nanocrystalline structure.

The XRD pattern of $CaF_2:Eu^{3+}$ phosphor for variable concentration of Eu^{3+} (1, 1.5 & 2.0mol%), which is depicted in **Fig 2.** There is no consider change in the peak position with the doping concentration of Eu^{3+} ion, the average crystallite size of the phosphors observed at 29.31 nm & the peak index exposed the cubic phase of CaF_2 phosphor. They are good accordance with JCPDS card no. 35-0816. It is indicated there is no other impurity phase that can be studied in the phosphor and from these experimental results, we can conclude that Eu^{3+}ions have been introduced in the host material CaF_2[37].

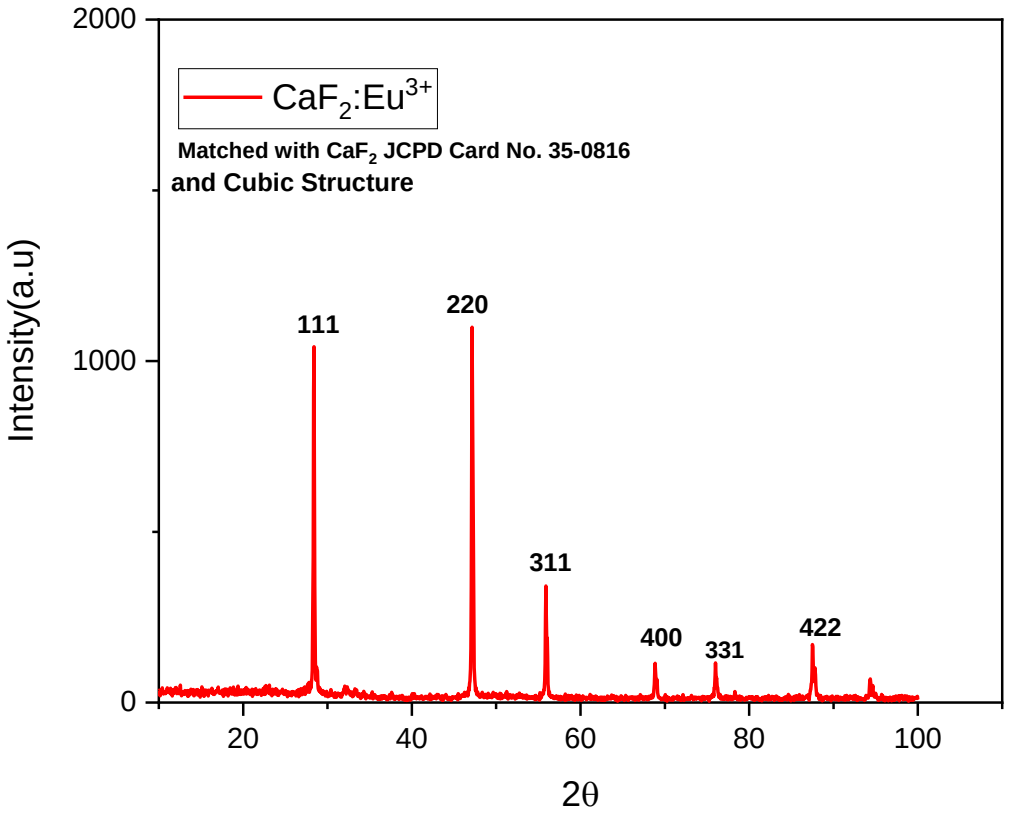

Fig.1(a): XRD pattern of $CaF_2:Eu^{3+}$phosphor for 1.5 mol%

Table 1. Crystallite Size

hkl	Peak Position(2θ)	FWHM	Crystallite Size D(nm)	Average Size D(nm)
111	28.25	0.005236	28.52	
220	47.40	0.006981	22.65	
311	55.70	0.006981	24.28	29.31 nm
400	68.65	0.005236	34.18	
331	76.20	0.006981	26.39	
422	87.55	0.005236	39.81	

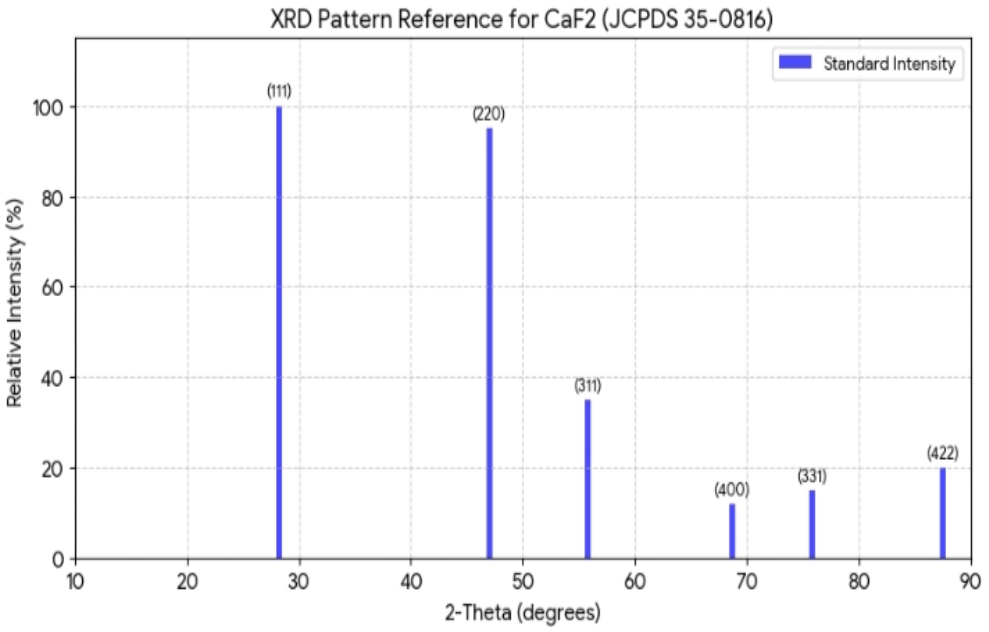

Fig.1(b) XRD pattern reference for CaF_2(JCPDS 35-0816)

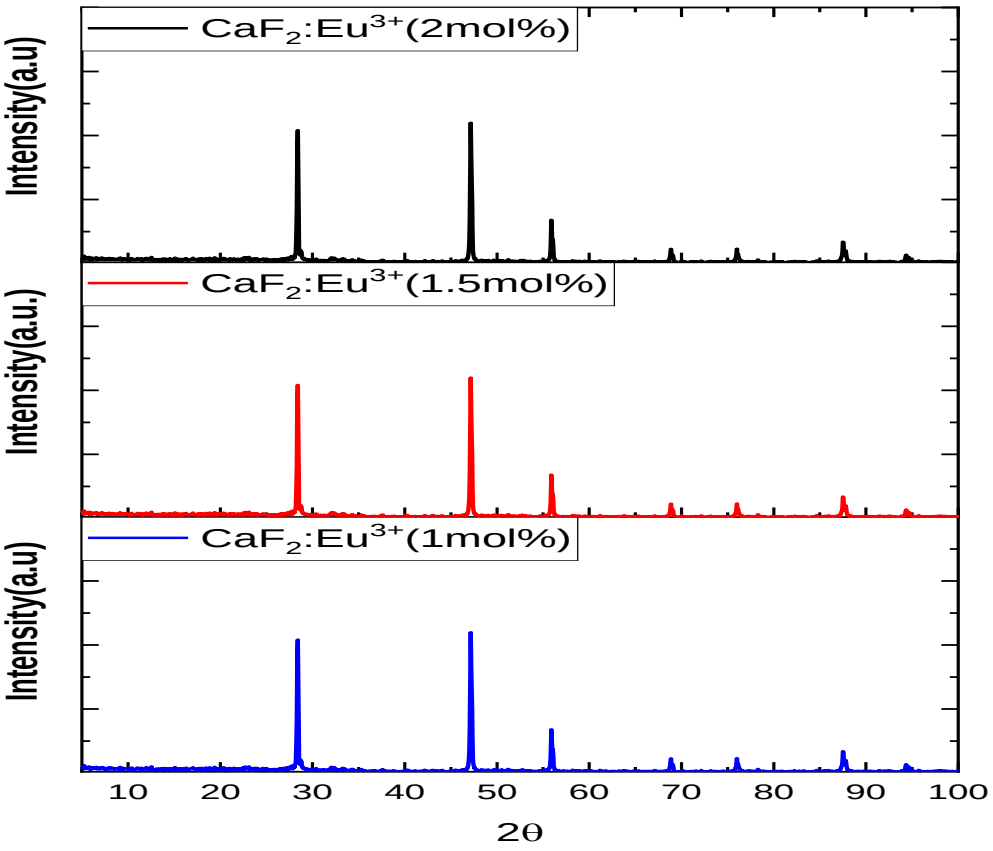

Fig. (2) XRD pattern of CaF_2:Eu^{3+}phosphor for 1.0,1.5 and 2.0mol%.

3.2 FTIR Analysis

FTIR spectrum of Eu^{3+} doped CaF_2 for 2.0 mol% shown in the Fig. (3) FTIR analysis of this phosphor has been performed at room temperature within the range of (500-3000) cm^{-1}. Some bundles appeared within of vibrational frequencies (500-3000) cm^{-1} which is (1639.01cm^{-1}, 1259.3,618.8 ,592) cm^{-1}. Frequency band 1639.9 cm^{-1} attributed H-O-H bending, 1259.3 cm^{-1} found due to C-O stretching and 618.8 and 592 cm^{-1} attributed to metal oxygen (Eu-O) vibration which is confirm Eu_2O_3 presence in the present phosphor, whereas the Ca-F lattice vibration of the host is massive "dip" at the far right. State clearly that the absence of other significant peaks confirms the high purity of the synthesized phosphor.

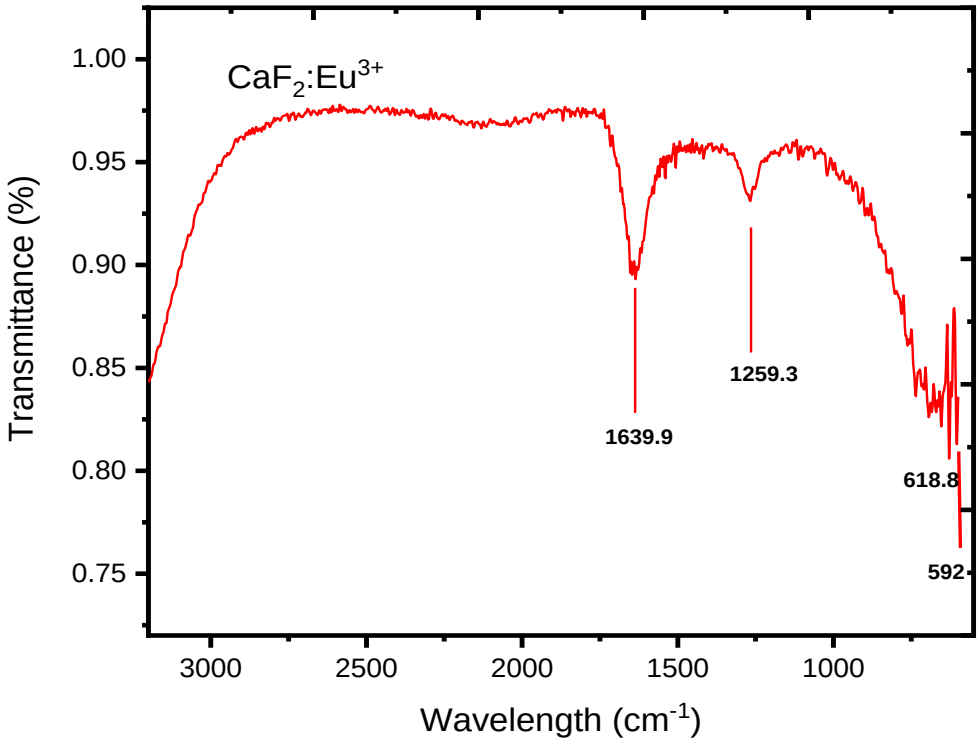

Fig. (3) FTIR Spectra of CaF_2:Eu^{3+} (2.0 mol%)

4. Luminescence properties

The prepared CaF_2: Eu^{3+} phosphor exhibits an orange-red emission attributable to the characteristic luminescence of Eu^{3+} ions, the excitation and emission spectra of CaF_2: Eu^{3+}, as shown in Fig. 4(a) and 4(b), reveal a broad excitation band observed around 280 nm in the ultraviolet region. Upon UV excitation, the absorbed energy is efficiently transferred to Eu^{3+} ions, leading to their characteristic sharp emission lines in the visible range. The main emission originates from the $^5D_0 \rightarrow {}^7F_j$ (j = 0–4) transitions. Between these, the $^5D_0 \rightarrow {}^7F_2$ electric dipole transition is the most prominent, giving rise to a strong red emission in the range of approximately 610–620 nm. This particular transition is highly sensitive to the local environment of Eu^{3+} ions and suggests that the ions occupy sites lacking inversion symmetry inside the

host lattice. In contrast, the $^5D_0 \rightarrow {}^7F_1$ magnetic dipole transition, typically observed near 590nm, is less sensitive to the surrounding environment and serves as a reference for symmetry analysis, in the emission spectra range of wavelength from 550 to 650 nm with prominent a high-intensity peak found at 611 nm resulting from energy transfer.

The emission characteristics of CaF_2: Eu^{3+} phosphor were analysed under excitation at 280 nm, the resulting spectrum exhibits distinct emission lines corresponding to the $^5D_0 \rightarrow {}^7F_j$ (J = 1, 2, and 3) transitions of Eu^{3+} ions., a strong emission peak observed at 611 nm is assign to the electric dipole transition from $^5D_0 \rightarrow {}^7F_2$, while the emission around 590 nm is associated with a forced magnetic dipole transition. Overall, the emission profile spans the 550–650 nm region, arising primarily from the $^5D_0 \rightarrow {}^7F_j$ (J = 1, 2) transitions. Furthermore, photoluminescence studies of CaF_2: Eu^{3+} phosphors reveal that the emission intensity of Eu^{3+} ions is highly dependent on their doping concentration. Initially, the intensity increases as the Eu^{3+} concentration rises from 1.0 mol% to 2.0 mol% due to the increase in luminescent centres. However noticeable significant decline in intensity observed when the concentration is increased to 2.5 mol% which is clear signature of concentration quenching. This phenomenon occurs because, at higher concentration, the distance between activator ions decreases, leading to non-radiative energy transfer through mechanism like cross-relaxation to quenching sites. Consequently ,2.0 mol% acts as the optimum concentration for maximum luminescence in this CaF_2 host, beyond which the efficiency of the phosphor diminishes.

The results suggest that Eu^{3+} ions occupy lattice sites of low symmetry within the CaF_2 host, as evidenced by the comparatively weaker magnetic dipole (MD) transition relative to the electric dipole (ED) transition. With increasing dopant concentration, particularly near 2.0 mol%, concentration quenching becomes prominent due to enhanced energy transfer between adjacent Eu^{3+} ions, resulting in observable shifts in emission peak positions. In view of these findings, CaF_2: Eu^{3+} phosphor with an optimal dopant concentration of approximately 2.0 mol% is considered a promising candidate for compact fluorescent lamp (CFL) applications when excited at 280 nm.

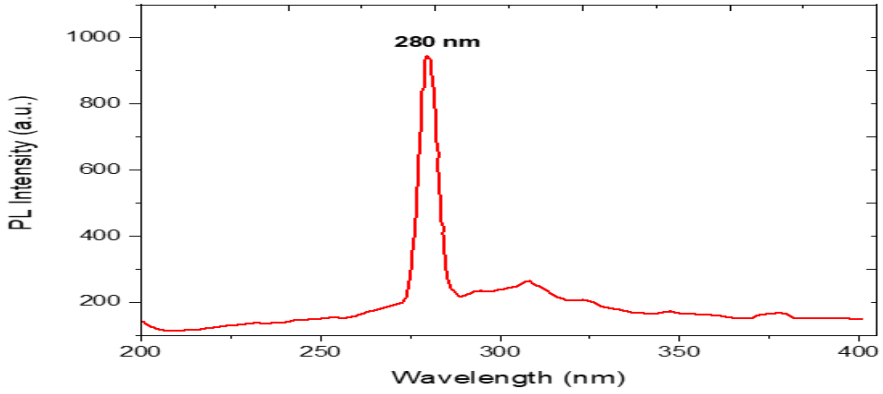

Fig. 4(a) PL excitation spectra of CaF_2:Eu^{3+}

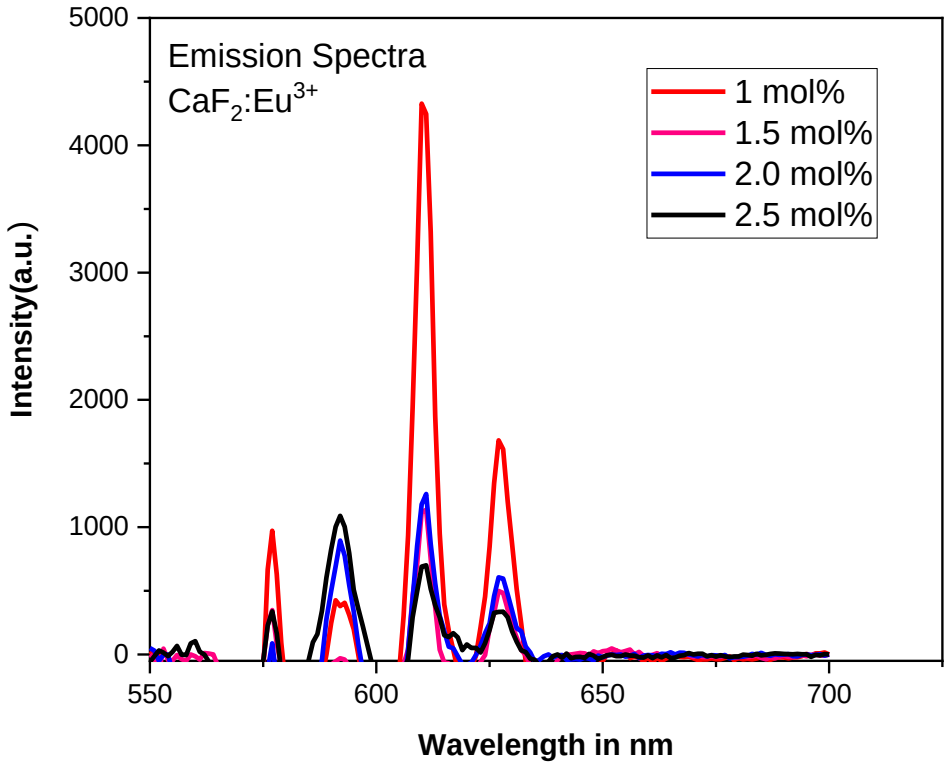

Fig. 4(b) PL emission spectra of $CaF_2:Eu^{3+}$ excitation at 280nm.

4.1 CIE Coordinates

The CIE 1931 chromaticity diagram for the Eu^{3+} doped CaF_2 phosphor serves as a vital tool for assessing its colorimetric performance, showing the precise coordinates of its light output, which is shown in Fig. (4c). When excited, typically by ultraviolet region, this phosphor exhibits characteristics emission peaks in the visible region, most prominently the orange red band at approximately 591 nm and 611 nm. The chromaticity coordinate for Eu^{3+} doped CaF_2 sample were derived using spectral energy distribution data obtained through spectrophotometric analysis. The resulting coordinates often lie near the edge of the red region (x=0.6474, y=0.3522), of this material. To determine the CIE coordinates of these phosphors, photoluminescence spectroscopy is employed. In this process, the emitted light is captured and directed through a monochromator, which separates it into individual wavelengths. The intensity at each wavelength is then recorded, and the overall spectral distribution is used to calculate the corresponding CIE coordinates.

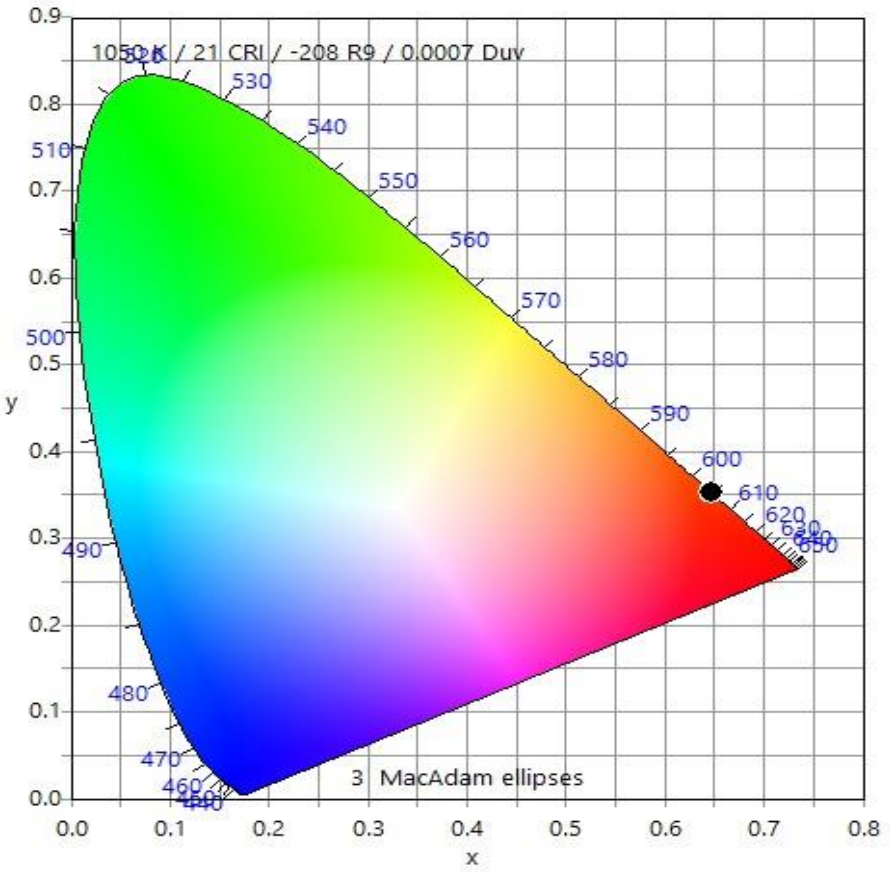

Fig.(4c) CIE Coordinate for $CaF_2:Eu^{3+}$ Phosphor for 1.5 mol%

5. Thermoluminescence (TL) Optimization

Thermoluminescence (TL) characteristics of Eu^{3+} doped calcium fluoride phosphors have attracted significant attention because of their possible application in radiation dosimetry due to the material's high sensitivity and stable lattice structure. The optimization of TL response in this material primarily depends on factors such as dopant concentration, synthesis conditions and post-preparation thermal treatment. As illustrated fig 5(a) the TL glow curve of Eu^{3+} doped CaF_2 phosphor for different concentration of Eu^{3+} ions (0.1 to 2.0 mol%). The intensity increases with increasing the concentration of Eu^{3+} up to 1.5 mol% then it decreases due to concentration quenching effect, the TL intensity shows a strong dependence on Eu^{3+} ion concentration peak intensity usually increases up to critical threshold (often around 0.1 to 1.5 mol%) beyond which concentration quenching occurs due to non-radiative energy transfer between closely speed of Eu ions.

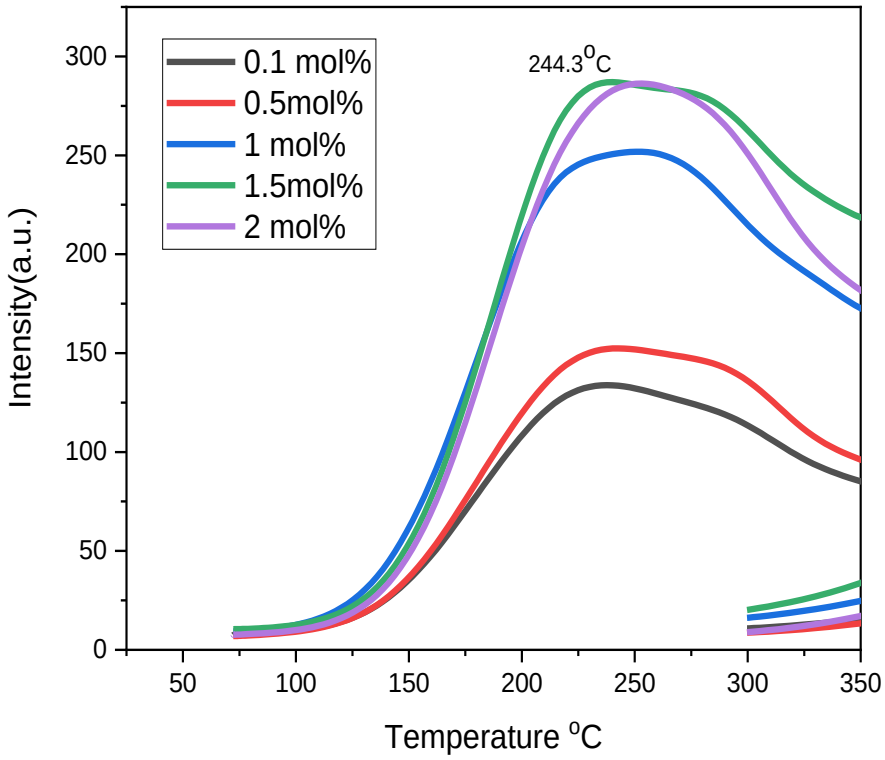

Fig. (5a) TL Glow Curve of $CaF_2:Eu^{3+}$ different concentration (0.1 to 2.0 mol%) at 0.1kGy Gamma Dose at heating rate 5^oCs^{-1}

5.1 TL Glow Curve Analysis

The glow curve shown in fig(5b) for Eu^{3+} dopes CaF_2 which is subjected to various (0.1 to 3.0 kGy) dose irradiation, this fig. depicts the behaviour of TL intensity as a function of gamma dose. It is observed from the figure; dose response shows a linear behaviour in the gamma dose region . The extreme intensity observed for 1.5 mol % of Eu^{3+} ion, after gamma irradiation a considerable deviation in the temperature of the TL glow curve peak as well as intensity was observed[38]. This may due to the reorganization of current existing trapping centre along with the formation of additional charge traps. In TL glow curve the primary temperature observed around 225°C to 240°C, which is depending upon the doping concentration and secondary low temperature may appear around 160°C to 180°C, which are typically associated with shallow traps and are prone to thermal fading. In TL glow curves under the different gamma irradiation dose (0.5 to 3.0 kGy) shows an increase of gamma doses, the shape of glow peak did not change significantly. For 0.5kGy dose a peak observed at temperature 230°C and for 1kGy dose peak observed at temperature 220.8 °C. A good T L dosimeter peak can be seen at 220.8°C as the TL intensity increases with Gamma exposure time (5b). This curve can be successfully theoretically and experimentally fitted using the CGCD method.[38]

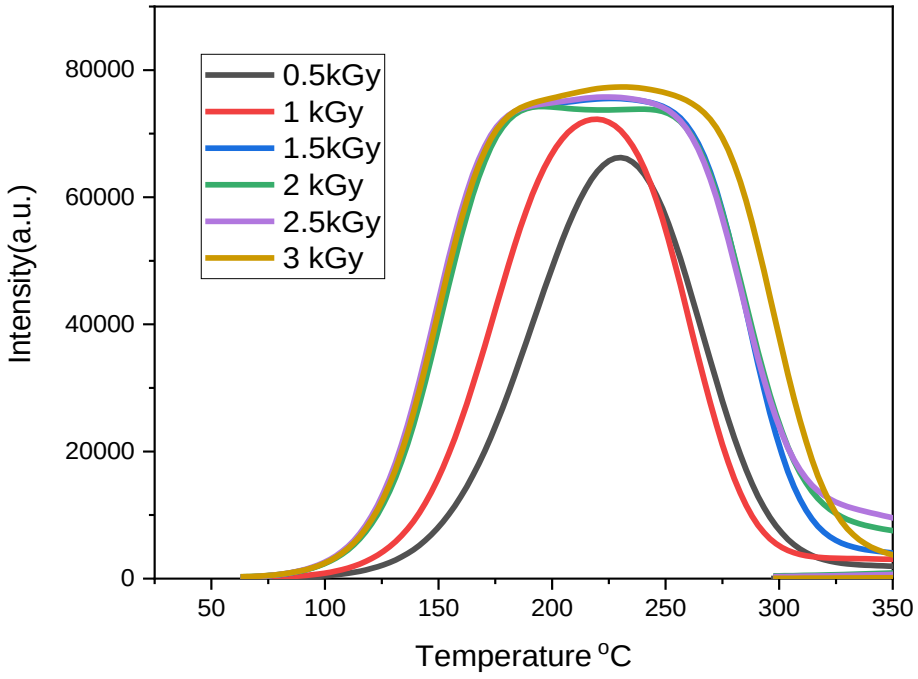

Fig(5b).TL glow curve of $CaF_2:Eu^{3+}$ (1.5 mol%) phosphor at variable gamma dose 0.5- 3.0 kGy at heating rate 5^oCs^{-1}

5.2 Determination of Kinetic Parameters using Initial Rise Method

Using the initial rise method, the activation energy (E_a) of the prepared phosphor was determined. In graph a plot of ln(I) vs 1/kT was obtained from the initial ascending part of the glow curve, the linear fitting of the experimental data yielded a slope of -0.706 corresponding to an activation energy of 0.706 eV, the high correlation coefficient ($R^2 = 0.987$) shows the reliability of the calculated kinetic parameter.

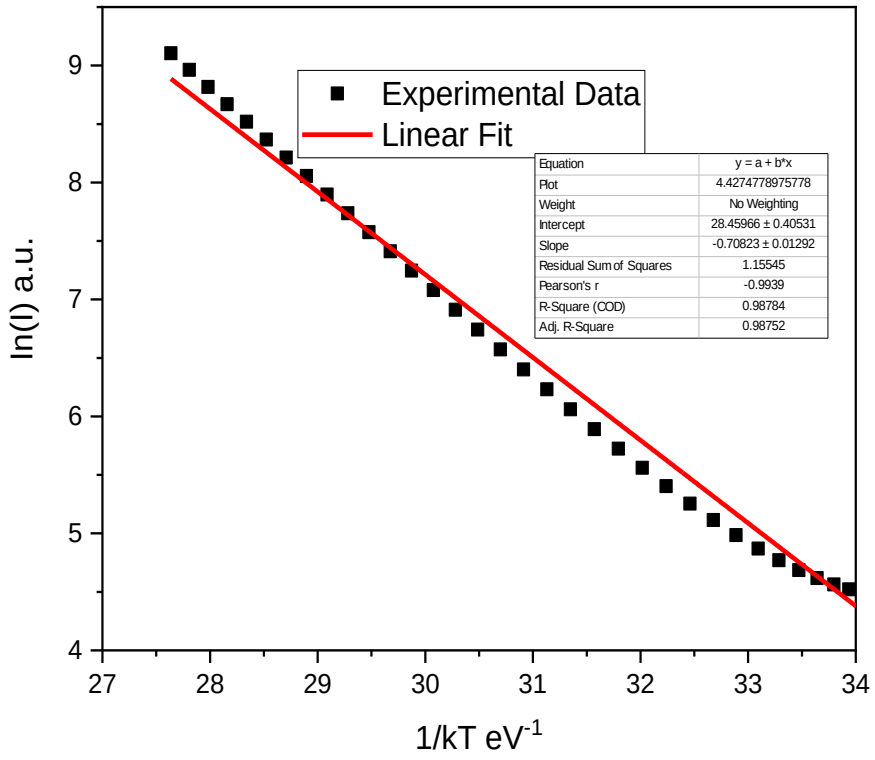

Fig.(5c) Plot of In (I) vs 1/kT for the initial rising part of the TL glow curve using the Initial Rise Method.

5.3 CGCD Glow Curve

The thermoluminescence properties Eu^{3+} doped CaF_2 phosphors are characterized by complex glow curve that typically exhibits multiple overlapping peaks, reflecting the presence of various trap level within the band gap. To separate overlapping peaks and evaluate critical trapping parameters such as activation energy (E), order of kinetics(b), and frequency factor(s), the Computerized Glow Curve Deconvolution (CGCD) technique was utilized. Specifically, the Glow Fit software was applied to analyze the 1 kGy gamma – irradiated curve[37]. Which is shown in the glow curve fig (5d), the kinetic parameters are determined using CGCD method. The CGCD fitting shows both narrow and deep traps contributing to the TL emission. The low temperature peaks are ascribed to shallow traps with lower activation energy, while at the higher temperature peaks correspond to deeper and more stable trapping centres responsible for dosimetry applications. The intensity of the main dosimetry peak increases significantly at 1 kGy, suggesting efficient charge carrier trapping. The dose lies within the linear response region of CaF_2 based phosphors good appropriateness for high-dose dosimetry. The obtained kinetic parameters such as activation energy and frequency factor further confirm the presence of thermally stable trapping center. The calculated geometric factor (μ) ranges from 0.46 to 0.52, since these values lie at 0.52, it indicates that the phosphor follows second-order kinetics and 0.46, 0.50 is general order kinetics or near second order kinetics. This suggests a significant probability of charge carriers undergoing re-trapping before radiative recombination occurs. The activation energy, which represents the energy required to release trapped electrons (trap depth), shows a descending trend across the samples moving from 1.264 eV to

0.512 eV. The kinetic parameters reveal that, the most stable dosimatric peak observed for peak 1 due to its high activation energy (1.264) and frequency factor (5.10 x $10^{11}s^{-1}$), these values suggested a long-life time & negligible thermal fading at ambient temperatures. Peak 2 and peak 3 exhibits lower activation energy (0.781 eV & 0.512eV) compare to peak 1 indicating they are shallow traps prone to rapid fading.

Fig.(5e) shows gamma dose vs intensity plot for $CaF_2:Eu^{3+}$ (1.5mol%) phosphor, we observed the variation of TL intensity as a function of gamma dose. It is study that the TL intensity increases with the increase in gamma dose from 0.1kGy to 3.0 kGy, which is followed a relatively slower rate of increase at higher doses indicating a trend towards saturation of the trapping centers.

The examination of thermoluminescence(TL) properties of the synthesized Eu^{3+} doped CaF_2 phosphors have significant potential for radiation dosimetry application, the high radiation sensitivity of the host material combined with efficient trap centers introduced by Eu doping enhance the TL output, making it highly practicable for low- dose radiation monitoring. Furthermore, a highly linear dose response range allows straightforward and precise dose evaluation without the requirement of complex calibration algorithms. Combined with its inherent thermal and mechanical stability, this phosphor exhibits crucial dosimetric attributes necessary for potential application in clinical radiation fields, personal safety monitoring and environmental dose assessments.

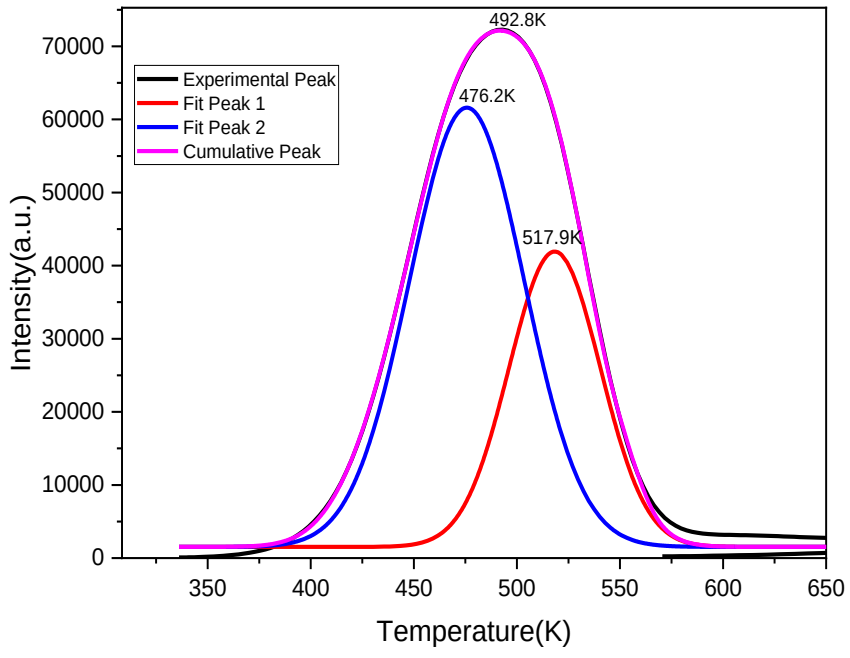

Fig. (5d) CGCD glow curve of $CaF_2:Eu^{3+}$ for 1kGy gamma dose.

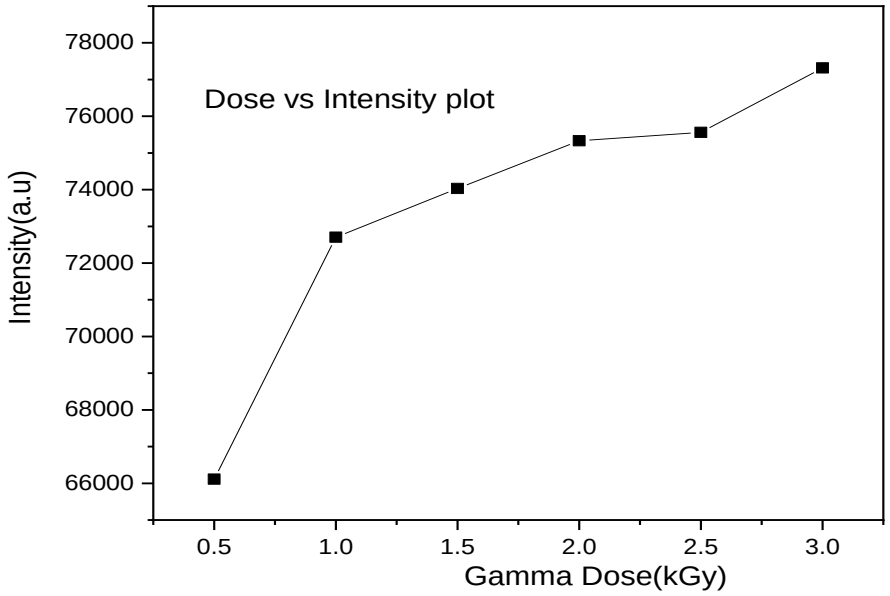

Fig.(5e) Gamma dose vs Intensity plot for $CaF_2:Eu^{3+}$ (1.5mol%)

Table.2 Details of Kinetic parameters TL glow curve of $CaF_2:Eu^{3+}$ at heating rate 5 $^oCs^{-1}$

Peak	T_1(K)	T_m(K)	T_2(K)	τ	δ	ω	μ = δ/ω	Activation Energy (Eav)	Frequency Factor
Peak1	492.2	517.9	546.7	25.8	28.8	54.6	0.52	1.264 ev	5.10×10^{11}
Peak2	442.4	476.2	510.6	33.8	34.4	68.2	0.50	0.781 ev	3.33×10^{7}

Table 3. Life Time and Fading.

Parameter	Peak 1(1.264 eV)	Peak 2 (0.781 eV)
Trap Depth	Deep Trap	Shallow Trap
Fading Rate	Very Low	High
Lifetime	Long (Years/Month)	Short (Days/Hours)
Application	Ideal for Dosimetry	Unstable for Storage

4.Comparison Table of Kinetic Parameters:

The table below summarizes the activation energy valued obtained for peak 2 using two different analytical methods:

Glow Peak	Method Used	Activation Energy(E in eV)	Difference(ΔE)
Peak 2 (T_m= 476.2K)	**Peak Shape Method**	**0.781 eV**	**0.075**
	Initial Rise Metod	**0.706 eV**	

To understand the trapping mechanism and defect centers responsible for the thermoluminescence (TL) emission in the prepared phosphor, the kinetic parameters activation energy (E) , frequency factor (s), and order of kinetics (μ) were observed. A comparative analysis was executed using two different methods, Chen's Peak Shape Method and the Initial Rise Method, focusing on the well resolved glow peak observed at 476.2 K (Peak 2), the geometric factor ($\mu_g = \delta/\omega$) obtained from the Peak Shape method was found to be 0.50, indicating that the trapping state obeys second-order kinetics and this implies a significant probability of re- trapping before recombination occurs. The activation energy (E) calculated using peak shape method which is found to be 0.781 eV, with a corresponding frequency factor (s) of $3.33 \times 10^7 s^{-1}$. To authenticate these results and remove any potential artifacts arising from the chosen kinetic order, the Initial Rise method was applied to the same glow peak and the Initial Rise method is highly reliable as it is a fundamentally independent of the order of kinetics, using only the low – temperature tail where trap emptying is negligible. The Arrhenius plot of ln(I) versus 1/kT yielded a linear fit with a slope corresponding to an activation energy (E) of 0.706 eV.

The activation energy values found from both methods show close agreement, with a minor change of approximately 0.075 eV, this slight understanding in the Initial Rise method is a well -documented phenomenon in TL analysis. It occurs because the initial Rise method avoids any experimental distortions or thermal bleaching effects that may impact the higher temperature side of the complete glow curve, the closeness of the trap depth values calculated from these independent theories confirm the accuracy, consistency, and reliability of the evaluated kinetic parameter for this phosphor material.

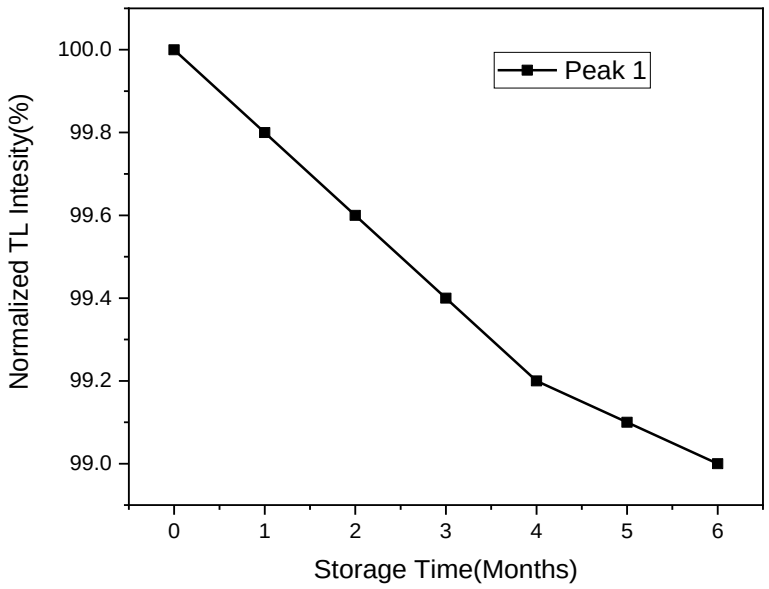

Fig.(5f) Fading characteristics of $CaF_2:Eu^{3+}$ phosphor for peak 1 stored at room temperature for six months.

6. Conclusion

- In conclusion Eu^{3+} doped CaF_2 phosphor has been successfully produced using the solid-state reaction route.
- A structural study of the $CaF_2:Eu^{3+}$ phosphor by XRD which is shows cubic phase structure and average crystallite size observed at 29.31nm and also FTIR characterization of this phosphor was done.
- Photoluminescence (PL) measurements of the prepared phosphor reveal an excitation peak cantered around 280 nm in the ultraviolet region. The emission spectrum displays broad bands at 591 nm, 611 nm, 625 and 650 nm. These emissions are attributed to electronic transitions from the $^5D_0 \rightarrow {}^7F_1$ (591 nm), and $^5D_0 \rightarrow {}^7F_2$ (611-625 nm), $^5D_0 \rightarrow {}^7F_3$(650nm) levels, the transition at 611 nm stand out the most dominant, providing the material is strong contribution leads to stable color output, producing orange-red emission. This strong emission profile makes its highly suitable for display technologies, including screen devices and monitors.
- In TL glow curve analysis , we observed that the intensity increases with increasing of dopant ions concentration under gamma doses. And peaks observed at temperature 244.3°C at heating rate 5^oCs^{-1}, Eu^{3+} doped CaF_2 phosphor for 1.5 mol% concentration of Eu^{3+} ion. After that, this 1.5mol% of Eu^{3+} ions irradiated with different gamma doses the peaks observed at temperature 220.8°C, showing a good TL dosimeter peak. The kinetic parameters such as order of kinetics frequency factor and activation energy that were calculated using initial rise method and peak shape method were fitted using CGCD technique. Gamma dose vs Intensity plot of this phosphor was also studies, which shows that intensity is a function of gamma dose.

- Because of its highly thermal stability, narrow emission bands and long luminescence lifetime Eu^{3+} doped CaF_2 phosphors serves as an excellent luminescent material. Such properties making it highly effective for several applications in optoelectronics, such as flat panel display and solid-state lighting, Medical and environmental professionals rely on these phosphors with linear dose responses are used to accurately monitor radiation exposure. The novelty of the present work lies in the development of a highly stable single peak thermoluminescence phosphor without requiring complex co-doping strategies. Unlike conventional fluorite dosimeters that suffer from severe fading due to shallow traps, the synthesized Eu^{3+}:CaF_2 exhibit high-temperature trap centers 244.3ºC, ensuring minimal thermal fading and prolonged data storage reliability. Significantly, the precise linearity confirmed by the CGCD technique over the investigated gamma dose range establishes this material as a robust, dual-mode framework suitable for both advanced radiation-sensing dosimeters and color-pure red components in WLEDs.

References

1. D. C. Celikel, Smart E-Textile Materials, in Advanced functional materials, ed. N. Tasaltin, P. S. Nnamchi and S. Saud, IntechOpen, London, 2020, pp. 1–16, DOI: 10.5772/ intechopen.92439.
2. L. Liu, W. Xu, Y. Ding, S. Agarwal, A. Greiner and G. Duan, A review of smart electrospunfibers toward textiles, Comput. Commun., 2020, j.coco.2020.100506. 22, 100506, DOI: 10.1016/ j.coco.2020.100506.
3. M. Ghahremani Honarvar and M. Latifi, Overview of wearable electronics and smart textiles, J. Text. Inst., 2017, 108(4), 631–652, DOI: 10.1080/00405000.2016.1177870.
4. M. Chen, Y. Ma, J. Song, C. F. Lai and B. Hu, Smart clothing: connecting human with clouds and big data for sustainable health monitoring, Mob. Netw. Appl., 2016, 21(5), 825–845, DOI: 10.1007/s11036-016-0745-1.
5. A. Bratovcic, Different applications of nanomaterials and their impact on the environment, Int. J. Mater. Sci. Eng., 2019, 5(1), 1–7, DOI: 10.14445/23948884/IJMSE-V5I1P101.
6. P. Kumar, S. Singh and B. K. Gupta, Future prospects of luminescent nanomaterial based security inks: from synthesis to anti-counterfeiting applications, Nanoscale, 2016, 8(30), 14297–14340, DOI: 10.1039/C5NR06965C.
7. J. Yu, M. Luo, Z. Lv, S. Huang, H. H. Hsu, C. C. Kuo and Y. Zhou, Recent advances in optical and optoelectronic data storage based on luminescent nanomaterials, Nanoscale, 2020, 12(46), 23391–23423, DOI: 10.1039/ D0NR06719A.
8. S. Kwon, Y. H. Hwang, M. Nam, H. Chae, H. S. Lee, Y. Jeon and K. C. Choi, Recent progress of fiber shaped lighting devices for smart display applications—a fibertronic perspective, Adv. Mater., 2020, 32(5), 1903488, DOI: 10.1002/adma.201903488.
9. M. Cinquino, C. T. Prontera, M. Pugliese, R. Giannuzzi, D. Taurino, G. Gigli and V. Maiorano, Light-emitting textiles: device architectures, working principles, and applications, Micromachines, 2021, 12(6), 652, DOI:10.3390/mil12060652.
10. X. Shi, Y. Zuo, P. Zhai, J. Shen, Y. Yang, Z. Gao and H. Peng, Large-area display textiles integrated with functional systems, Nature, 2021, 591(7849), 240–245, DOI: 10.1038/ s41586-021-03295-8.
11. M. Haque, Nanofabrics in the 21st century: a review, Asian J. Nanosci. Mater., 2019, 2(2), 131–148, DOI: 10.26655/ ajnanomat.2019.3.2.

12. Z. Gong, Z. Xiang, X. OuYang, J. Zhang, N. Lau, J. Zhou and C. C. Chan, Wearable fiber optic technology based on smart textile: a review, Materials, 2019, 12(20), 3311, DOI: 10.3390/ ma12203311.
13. C. W. Kan and Y. L. Lam, Future trend in wearable electronics in the textile industry, Appl. Sci., 2021, 11(9), 3914, DOI: 10.3390/app11093914.
14. A. Angelucci, M. Cavicchioli, I. A. Cintorrino, G. Lauricella, C. Rossi, S. Strati and A. Aliverti, Smart textiles and sensorized garments for physiological monitoring: a review of available solutions and techniques, Sensors, 2021, 21(3), 814, DOI: 10.3390/s21030814.
15. X. Hu, Y. Dou, J. Li and Z. Liu, Buckled structures: fabrication and applications in wearable electronics, Small, 2019, 15(32), 1804805, DOI: 10.1002/smll.201804805.
16. Q. Zhang, Y. L. Wang, Y. Xia, P. F. Zhang, T. V. Kirk, X. D. Chen and X. D, Textile-only capacitive sensors for facile fabric integration without compromise of wearability, Adv. Mater. Technol., 2019, 4(10), 1900485, DOI: 10.1002/admt.201900485.
17. A. A. Simegnaw, B. Malengier, G. Rotich, M. G. Tadesse and L. Van Langenhove, Review on the integration of microelectronics for E-Textile, Materials, 2021, 14(17), 5113, DOI: 10.3390/ma14175113.
18. E. A. Hassan, M. A. Ahmed, S. Zhu and O. K. Alebeid, Fibre based wearable electronic technology for personal protective clothing, in Protective textiles from natural resources, Woodhead Publishing, 2022, pp. 511–547, DOI: 10.1016/ B978-0-323-90477-3.00019-5.
19. A. A. Basheer, Advances in the smart materials applications in the aerospace industries, Aircr. Eng. Aerosp. Technol., 2020, 92(7), 1027–1035, DOI: 10.1108/AEAT-02-2020-0040.
20. A. Raza, U. Hayat, T. Rasheed, M. Bilal and H. M. Iqbal, “Smart” materials-based near-infrared light-responsive drug delivery systems for cancer treatment: a review, J. Mater. Sci. Technol., 2019, 8(1), 1497–1509, DOI: 10.1016/ j.jmrt. 2018.03.007.
21. C. Mendes-Felipe, J. Oliveira, I. Etxebarria, J. L. Vilas-Vilela and S. Lanceros-Mendez, State-of-the-art and future challenges of UV curable polymer-based smart materials for printing technologies, Adv. Mater. Technol., 2019, 4(3), 1800618, DOI: 10.1002/admt.201800618.
22. Z. Li, F. Yang and Y. Yin, Smart materials by nanoscale magnetic assembly, Adv. Funct. Mater., 2020, 30(2), 1903467, DOI: 10.1002/adfm.201903467.
23. R. Priya, S. Kaur, U. Sharma, O. P. Pandey and S. J. Dhoble, A review on recent progress in rare earth and transition metals activated SrY_2O_4 phosphors, J. Mater. Sci.: Mater. Electron.
24. S. P. Ghorpade, R. H. Krishna, R. M. Melavanki, V. Dubey and N. R. Patil, Effect of Eu^{3+} on optical and energy bandgap of SrY_2O_4 nanophosphors for FED applications, Optik, 2020, 208, 164533, DOI: 10.1016/j.ijleo.2020.164533.
25. D. R. Taikar, Synthesis and luminescence property of SrY_2O_4:M (M= Eu^{3+}, Tb^{3+}, Sm^{3+} Tb3+, Sm^{3+}, Ce^{3+}, Bi^{3+}) phosphors, J. Lumin., 2018, 204, 24–29, DOI: 10.1016/ j.jlumin.2018.07.040.
26. E. Pavitra, G. S. R. Raju, W. Park and J. S. Yu, Concentration and penetration depth dependent tunable emissions from Eu^{3+} co-doped SrY_2O_4:Dy^{3+} nanocrystalline phosphor, New J. Chem., 2014, 38(1), 163–169, DOI: 10.1039/C3NJ00987D.
27. R.K. Tamrakar and K. Upadhyay, Combustion synthesis and luminescence behaviour of the Tb^{3+} doped SrY2O4 phosphor, J. Electron. Mater., 2018, 47(1), 651–654, DOI: 10.1007/s11664-017-5825-x.

28. S. P. Ghorpade, N. Kottam, R. Melavanki and N. R. Patil, Photoluminescence, TGA/DSC and photocatalytic activity studies of Dy^{3+} doped SrY_2O_4 nanophosphors, RSC Adv., 2020, 10(36), 21049–21056, DOI: 10.1039/D0RA03094E.
29. V. Singh, K. Swapna, S. Kaur, A. S. Rao and J. L. Rao, Narrow band UVB-emitting Gddoped SrY_2O_4 phosphors, J. Electron. Mater., 2020, 49(5), 3025–3030, DOI: 10.1007/s11664-020 08032-x.
30. R. Wei, Z. Zheng, Y. Shi, X. Peng, H. Wang, X. Tian and H. Guo, Tunable emission with excellent thermal stability in single-phased SrY_2O_4: Bi^{3+}, Eu^{3+} phosphors for UV LEDs, J. Alloys Compd., 2018, 767, 403–408, DOI: 10.1016/ j.jallcom.2018.07.101.
31. S. Bhatia, R. Priya, D. Kumar, S. Upadhyay and O. P. Pandey, Structural and luminescent studies of titanium co-doped SrY_2O_4:Eu phosphors, Luminescence, 2022, 37(9), 1585 1596, DOI: 10.1002/bio.4335.
32. I. Suryawanshi, R. Kalia, R. K. Kunchala, S. L. Mudavath and B. S. Naidu, Detection of latent fingerprints using luminescent $Gd_{0.95}Eu_{0.05}PO_4$ nanorods, J. Rare Earths, 2022, 40(4), 572–578, DOI: 10.1016/j.jre.2021.01.015.
33. S. P. Singh, S. Srinidhi, R. K. Kunchala, R. Kalia, S. N. Achary and B. S. Naidu, Structural and excitation-dependent photoluminescence properties of $Bi_{0.95x}Gd_xEu_{0.05}PO_4(0 \leq x \leq 0.95)$ solid solutions and their anticounterfeiting applications, Cryst. Growth Des., 2021, 21(8), 4619–4631, DOI: 10.1021/acs.cgd.1c00467.
34. I. Suryawanshi, S. Srinidhi, S. Singh, R. Kalia, R. K. Kunchala, S. L. Mudavath and B. S. Naidu, Downshifting and upconversion dual mode emission from lanthanide doped GdPO4 nanorods for unclonable anti counterfeiting, Mater. Today Commun., 2021, 26, 102144, DOI: 10.1016/j.mtcomm.2021.102144.
35. I. Pushpendra, R. K. Kunchala, S. N. Achary and B. S. Naidu, NaBi0.9Eu0.1(MoO4)2 nanomaterials: tailoring the band gap and luminescence by La^{3+} substitution for light-emitting diodes, ACS Appl. Nano Mater., 2019, 2(9), 5527–5537, DOI: 10.1021/acsanm.9b01111.
36. I. Pushpendra, R. K. Kunchala, S. N. Achary, A. K. Tyagi and B. S. Naidu, Rapid, room temperature synthesis of Eu^{3+} Doped NaBi(MoO4)2 nanomaterials: structural, optical, and photoluminescence properties, Cryst. Growth Des., 2019, 19(6), 3379–3388, DOI: 10.1021/acs.cgd.9b00267.
37. Neha Tiwari, R. K. Kuraria and S. R. Kuraria, "Effect of variable trivalent europium concentration on photo- and thermoluminescence of zirconium dioxide nanophosphors," Optik, 2015, 126(19), 2191-2195. DOI: 10.1016/j.ijleo.2015.05.086
38. Y.Parganiha, J. Kaur, V. Dubey, R. Shrivastava, and D. Chandrakar, “Violet blue emission and thermoluminescence glow curve analysis of Gd_2SiO_5 : Ce^{3+} phosphor” ,Optik, 2016 ,vol.127,no. 15, pp. 6243-6252